3D negative electrode stacks for integrated all-solid-state lithium-ion microbatteries

Please check the document version of this publication:

• A submitted manuscript is the version of the article upon submission and before peer-review. There can be important differences between the submitted version and the official published version of record. People interested in the research are advised to contact the author for the final version of the publication, or visit the DOI to the publisher's website.
• The final author version and the galley proof are versions of the publication after peer review.
• The final published version features the final layout of the paper including the volume, issue and page numbers.

Link to publication

Download date: 04. Oct. 2023

3D negative electrode stacks for integrated all-solid-state lithium-ion microbatteries

Loïc Baggetto,[*a] Harm C. M. Knoops,[bc] Rogier A. H. Niessen,[d] Wilhelmus M. M. Kessels[b] and Peter H. L. Notten[ad]

The deposition feasibility and electrochemical evaluation of highly structured negative electrode stacks for 3D-integrated batteries is demonstrated. The stacks comprise a TiN thin film, serving as both current collector and Li-barrier layer, covered by a polycrystalline Si (poly-Si) thin film as electrode material. In comparison with planar films, these poly-Si films present a storage capacity increase of about 5× for the highest pore aspect ratio electrodes. The step coverage of poly-Si can be considerably improved by growing TiN and poly-Si into wide trenches. This results in much smoother poly-Si films and significantly improved step coverage. Further optimization of the trench dimensions should result in poly-Si films with a Li-storage capacity increase of more than one order of magnitude with respect to planar films.

Introduction

The technological progress of the past few decades has been fuelled by research advances related to device miniaturization. The development of energy storage devices with higher energy- and power-density largely contributed to this progress.[1] Rechargeable lithium-ion batteries have become a crucial player for enabling increasing miniaturization and mobility, as demonstrated by the market predominance of this battery type in many portable applications.[1,2] It has been identified that a next step of miniaturization can consist of integrating these devices directly onto microchips.[2,3]

Various lithium-ion microbattery concepts have been presented, however, only planar solid-state thin-film batteries have so far successfully emerged the pilot production phase.[3,4] Although these batteries have several advantages over liquid-based Li-ion batteries, they also present several drawbacks, such as the low melting temperature of pure Li electrodes and the limited storage capacity resulting from the planar substrate configuration.[3,4] These drawbacks can be alleviated by making use of the third dimension of the substrate material and by adopting novel electrode chemistries. Recently, several 3D microbattery concepts have been proposed[3–9] and only a few of these concepts are focusing on the achievement of full solid-state 3D microbatteries.[3,5,7]

The concept of 3D integrated all-solid-state microbatteries was recently disclosed[3] and a planar negative electrode stack comprising a silicon electrode was thoroughly evaluated as a test structure.[4,9] As a next step towards achieving a highly structured battery prototype, the preparation and characterization of a 3D negative electrode stack deposited into porous structures, e.g. high aspect ratio pores and trenches, will be discussed in this publication. Achieving such 3D negative electrode stacks requires the combination of advanced processing techniques, such as the etching of the substrate material to enlarge the effective surface area of the battery, and the step conformal deposition of thin layers inside the created 3D structures.[3] Although the processing of 3D structures into Si has become more or less standard by means of reactive ion etching (RIE),[10] the preparation of uniform layers into 3D structures requires appropriate deposition processes, such as atomic layer deposition (ALD) and low pressure chemical vapour deposition (LPCVD).[3]

In the present study, a substrate geometry consisting of pores was first adopted. Subsequently, ALD was employed for growing 60 nm thick layers of titanium nitride (TiN), a material which has been recently studied as a potential Li-barrier and current collector.[4,9,11,12] Next, LPCVD was used for depositing 50 nm thick films of polycrystalline silicon (poly-Si) onto TiN. Poly-Si was chosen because of its suitable properties as a negative thin film electrode material.[4,9] In order to investigate the step coverage of the deposited materials, the resulting 3D stacks were characterized with high resolution scanning electron microscopy (HRSEM). To understand the impact of the substrate morphology on the grown materials, additional experiments were conducted. The morphology of individual TiN layers prepared inside pores and of TiN/poly-Si stacks deposited inside trenches was also investigated. The electrochemical properties of 3D negative electrodes prepared inside pores were investigated by means of electrochemical galvanostatic cycling in order to measure the increase in storage capacity of the 3D negative electrode stacks. Furthermore, the capacity degradation upon cycling was investigated by SEM and found to be caused by the solid electrolyte interphase (SEI) growth.

[a]Department of Chemical Engineering and Chemistry, Eindhoven University of Technology, P.O. Box 513, 5600MB Eindhoven, The Netherlands. E-mail: l.baggetto@tue.nl; Tel: (+31) 4027 46247
[b]Department of Applied Physics, Eindhoven University of Technology, P.O. Box 513, 5600MB Eindhoven, The Netherlands
[c]Materials innovation institute M2i, 2600GA Delft, The Netherlands
[d]Philips Research Laboratories, High Tech Campus 4, 5656AE Eindhoven, The Netherlands
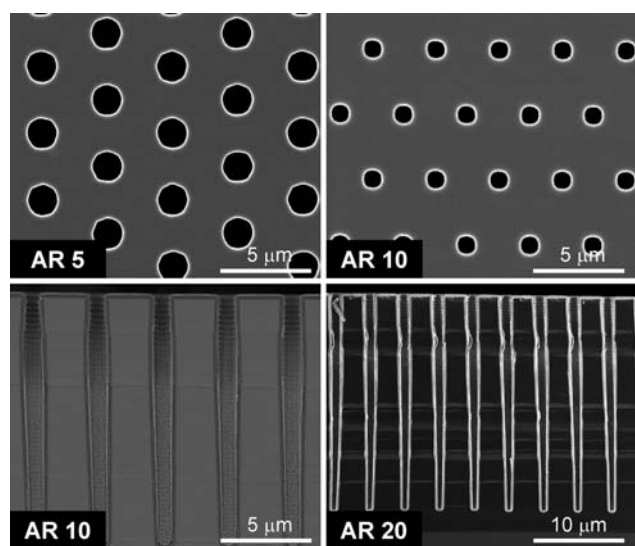
Experimental

(100) oriented silicon was used as starting material. In order to increase the effective surface area of the Si substrates, etching of pores with aspect ratios of 5, 10 and 20 and trenches of aspect ratio 5 was conducted using photolithography and RIE parameters published previously.[10] After thermal oxidation of the substrates etched with pores, the different samples were used as a supporting material for the subsequent depositions of TiN and poly-Si thin films. Remote plasma ALD using Oxford Instruments FlexAL™ was employed to grow 60 nm thick TiN films. The TiN process conditions were described in previous works.[11–13] LPCVD poly-Si 50 nm thick films were grown on top of samples covered by TiN all in one deposition run and using the same conditions described in detail elsewhere.[4] Finally, the substrates were laser cut to the dimension required for the electrochemical cell.

The samples were analyzed with HRSEM using a Philips Nova 200 Nanolab Small Dual Beam and FEI Quanta3D FEG. For the electrochemical evaluation of the poly-Si thin-films storage capacity, a temperature controlled (25 °C) three-electrode cylindrical electrochemical cell was used. The liquid electrolyte, comprising 1 M LiPF$_6$ dissolved in EC–DMC–DEC (2 : 2 : 1 weight ratio), was provided by Puriel, Techno, Semichem Co., Ltd, Korea. Galvanostatic cycling was performed on a M4300 galvanostat (Maccor, Tulsa, USA) from 0 to 3 V $vs.$ Li/Li$^+$ at a low current density of 25 µA per cm^2 footprint area. Due to the pore and trench distributions only pores of aspect ratios 10 and 20 were measured electrochemically.

Results and discussion

3D pores covered with TiN and poly-Si layers are shown in the HRSEM photographs of Fig. 1. The dimensions of the pores measured from the photographs are listed in Table 1. It is known that the surface area enlargement increases with increasing pore

Table 1 Dimensions and expected surface area enlargement factors for pore structures of aspect ratios 5, 10 and 20. d represents the pore diameter, h the pore height and H_p and V_p the horizontal and vertical pitches, respectively. The area enlargement factors presented in the table are calculated using Eq. (1) presented elsewhere.[9]

Nominal aspect ratio	d/µm	h/µm	H_p/µm	V_p/µm	Measured aspect ratio	Area enlargement factor
5	1.8	8.4	3.5	3.5	4.7	4.9
10	1.0	13.8	3.5	3.5	12.5	4.5
20	1.1	21.7	3.5	3.5	19.7	7.1

diameter, pore height and with decreasing the structure pitch (repetition).[9] Here, the pores of aspect ratio 5 have a wider opening (1.8 µm) than the others. As a result, the area enlargement factor for the aspect ratio 5 pores is higher than that of the pores with aspect ratio 10.

Different locations inside the pores were inspected at higher magnifications. Similar film morphologies were found for TiN and poly-Si grown inside the pores of various aspect ratios. Fig. 2 shows the HRSEM photographs for pores of aspect ratio 10 (a) and 20 (b). On the top surface, continuous films are formed. At the entrance of the pores both materials show uniform layers, however, it is clear that poly-Si is composed of fine crystalline grains and reveals a so-called 'island-like' morphology. Moreover, it is evident that the thickness of both layers decreases at the
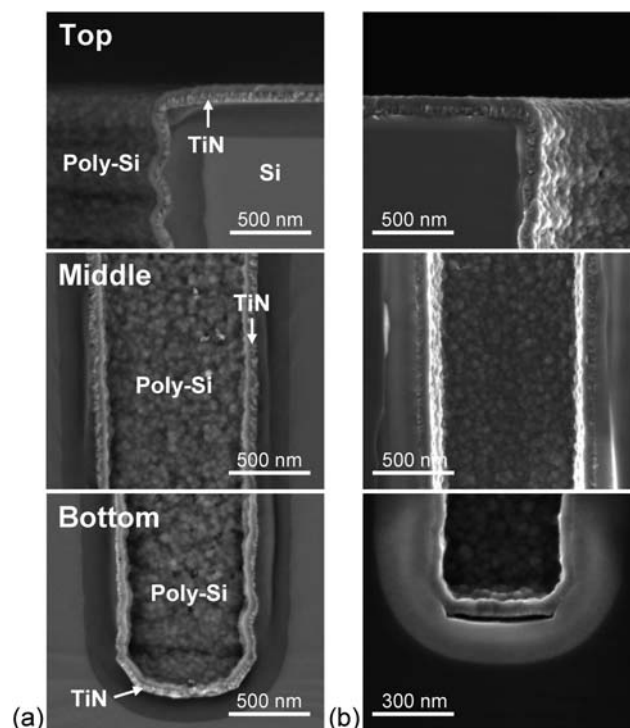

Fig. 1 HRSEM photographs of pore structures covered by ALD TiN and LPCVD poly-Si, showing top surface and cross-sections for various aspect ratio pores (AR). Note the different magnifications.

Fig. 2 HRSEM photographs showing the SiO$_2$-covered Si substrate covered by ALD TiN and LPCVD poly-Si thin-films for a pore of aspect ratio 10 (a) and 20 (b), at the top, middle and bottom of the pores. The layers are indicated on the aspect ratio 10 pore but are similar for the aspect ratio 20 pore. Note that the crack visible at the bottom of the aspect ratio 20 pore (b) results from the sample cleavage.
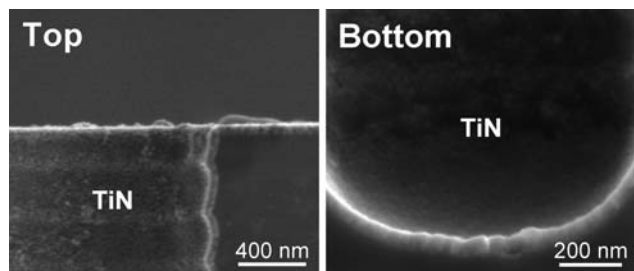
Table 2 Thicknesses (nm) for TiN and poly-Si layers, at different locations (top surface, entrance, middle and bottom of pore/trench) of the structures, measured during the HRSEM inspection

Material	Structure/Nominal aspect ratio	Top surface	Entrance	Middle	Bottom
TiN	Pore/5	58	53	44	34
TiN	Pore/10	60	48	46	40
TiN	Pore/20	55	58	45	18
TiN	Trench/5	60	49	46	47
poly-Si	Pore/5	54	40	29	23
poly-Si	Pore/10	52	43	28	30
poly-Si	Pore/20	56	48	37	31
poly-Si	Trench/5	53	45	46	45

entrance of the pores as compared to the top surface layer thickness. Going deeper into the pores, the layers are thinning down and reach their minimal thickness near the bottom of the structure.

The layer thicknesses measured for poly-Si and TiN at different locations of the pores are reported in Table 2. The step coverage for TiN is rather good for pores of aspect ratio up to 12.5 (nominal aspect ratio 10) with achieved step coverages of more than about 65%. For the deepest pores, the TiN deposition is more severely limited as only 18 nm is present at the bottom. In comparison with trenches, this limitation can result from limited in-pore diffusion of both $TiCl_4$ and plasma radicals.[12] The lower step coverage of TiN grown into high aspect ratio pores can also be attributed to the etching and poisoning of the growing material by HCl, which is produced during the ALD reactions, or to the plasma radical recombination at the surface of the pores. Surface recombination would result in a reduced flux of reactive plasma species inside the pores, thereby reducing the TiN layer growth as the ALD reactions no longer take place under satu-rated conditions.[11,12,14] In order to improve the step coverage of TiN for pore structures, longer dosing times for the precursor and plasma exposure steps might be required. A forthcoming publication will focus on the issues of attaining higher step coverage for remote plasma ALD processes.

The step coverage for poly-Si is about 60% (30 nm) for all aspect ratios independent of the diameter and depth of the pores. This indicates that reactant transport is not a limitation and that the growth of poly-Si is controlled by the surface kinetics. The surface morphology of the underlying layer is probably respon-sible for poly-Si non-uniformity. The surface morphology and chemistry may also have an impact on the nucleation mechanism of poly-Si and the lower amount of deposited material might thus
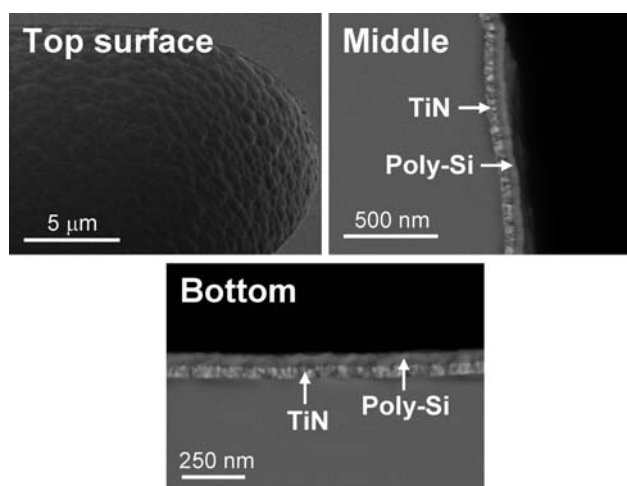
be due to some nucleation-delay effects. In order to investigate these hypotheses, pores covered by an individual TiN layer were inspected with SEM.

Fig. 3 shows HRSEM photographs of a TiN layer deposited inside pores of aspect ratio 11. It is clear that the morphology of the TiN layer grown onto RIE etched substrates is rather rough and is characterized by small grains throughout the pore. Poly-Si, which is grown onto these TiN-covered substrates, will con-formally follow the roughness of the TiN layer. As the amount of deposited poly-Si is low (the deposition was calibrated for a layer thickness of 50 nm), the conformal deposition of poly-Si will result in the formation of a non-uniform film, as observed in Fig. 2. If the deposition had been run for a longer period of time, it could be expected that the islands of poly-Si would gather and lead to the formation of a continuous layer. Indeed, much more uniform poly-Si films of larger thickness (about 0.4 μm) were created into very high aspect ratio pores (up to aspect ratio 50) of similar diameter opening. Using the same deposition conditions, uniform poly-Si films could be deposited onto thermally-grown SiO_2.[10] Therefore, it can be assumed that the difference in chemistry or surface roughness onto which poly-Si nucleates explains the observed 'island-like' morphology.

In order to further investigate the impact of the underlying substrate morphology on the step coverage and morphology of poly-Si films, wide trenches of aspect ratio 5 were prepared and covered by TiN and poly-Si thin films. The HRSEM photo-graphs corresponding to a single trench are shown in Fig. 4. Compared to the pore structure, the deposited poly-Si film is smoother and shows larger grains. This increase in poly-Si smoothness probably results from the lower roughness of the underlying TiN as a consequence of the growth of TiN onto a smoother substrate surface. It could also be that the nucleation and growth mechanism of TiN onto Si results in the formation of smoother TiN films (in contrast to the nucleation and growth mechanism of TiN onto SiO_2-covered Si substrates). The step coverage is greatly enhanced in comparison with the deposition inside pores. A decrease in layer thickness is also observed at the entrance of the trench but there is almost no variation in

Fig. 3 HRSEM photographs showing the top and bottom of a pore of aspect ratio 11 covered by ALD TiN. Note the different magnifications.
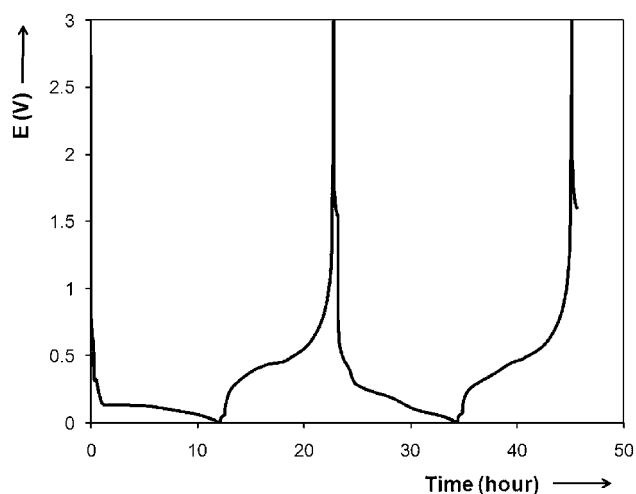

Fig. 4 HRSEM photographs showing a Si substrate covered by ALD TiN and LPCVD poly-Si thin-films for a trench of aspect ratio 5, at the top, middle and bottom of the trench. Note the different magnifications.
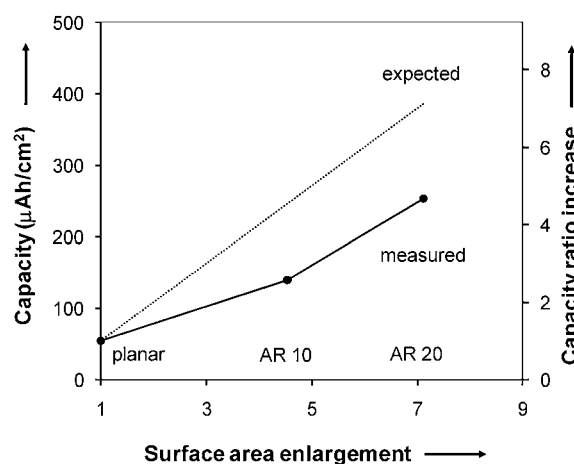
thickness from the entrance until the bottom of the structure (*cf.* Table 2). For pores having the same aspect ratio, a clear decrease of the layer thickness was observed from the top to the bottom of the structure. For these trenches, however, this does not occur. In the case of TiN, it is known that trenches can be much more easily covered than pores, due to faster in-trench diffusion of reactants.[12] For poly-Si, step coverage of 85% is now obtained, which corresponds to a substantial increase compared to what was deposited inside pores (60%).

The pore samples of aspect ratio 10 and 20 were measured electrochemically at low current. The resulting electrochemical potential profiles are presented in Fig. 5. These potential profiles are characteristic Li-ion insertion/extraction into/from Si electrodes.[4,9] Obviously, full crystallization of Si into $Li_{15}Si_4$ did not occur as a wide plateau during charging (Li-ion extraction) is absent. This probably results from the non-uniformity of the poly-Si layer. Indeed, it could well be that the uniform Si layer present at the top surface and at the top of the pores crystallizes while the rest of the layer, which is composed of smaller grains, cannot achieve long range ordering. Nevertheless, the observation of the partial crystallization into $Li_{15}Si_4$ indicates that the storage capacity of the poly-Si films is very close to the maximum theoretical value.

The capacities measured during the first charge and the expected storage capacities, as well as the corresponding capacity ratio increase, are plotted as a function of the surface area enlargement factor in Fig. 6. The calculated storage capacities are all based on the top surface layer thickness and assuming uniform poly-Si deposition inside the pores. The measured storage capacities are approximately 34 and 43% less than expected for the aspect ratio pores of 10 and 20 at values of about 140 and 255 µA h cm^{-2}, respectively. It should be noted that the calculation for the area enlargement factor is based on a geometrical configuration consisting of straight pores.[9] However, as observed from Fig. 2, it is clear that the pores are narrower at their bottoms as the depth becomes larger. Indeed, the pores are about 0.8 and 0.55 µm wide at the bottom for aspect ratio 10 and 20, respectively. As a result, the area enlargement

Fig. 6 Expected and measured reversible Li-ion storage capacities and capacity ratio increase of poly-Si thin films during the first cycle as a function of the surface area enlargement. The expected storage capacities are calculated assuming a homogeneous layer thickness equal to the top surface layer thickness.

calculation overestimates the real area enlargement. Moreover, although relatively low currents were employed during the electrochemical measurements (25 µA cm^{-2}, which corresponds to less than C/10 rate for the aspect ratio 20 pore electrode), the role of geometrical hindrance to Li-ion transport inside the pores cannot be excluded.[15] Furthermore, it is clear from the HRSEM inspection that poly-Si did not grow uniformly inside the pores as only about 56 and 61% of the expected thickness is found the aspect ratio 10 and 20 pores, respectively (*cf.* Table 2). These reasons explain the deviation between measured and expected capacity values. Nevertheless, the poly-Si films deposited inside the narrow pores with aspect ratio 20 show a large increase of the storage capacity by a factor of about 5 compared to planar films.

The cycle life of poly-Si films deposited in aspect ratio 10 and 20 pores is plotted in Fig. 7. The cycle life reveals a rapid decline after about 20 cycles. Although planar poly-Si electrodes
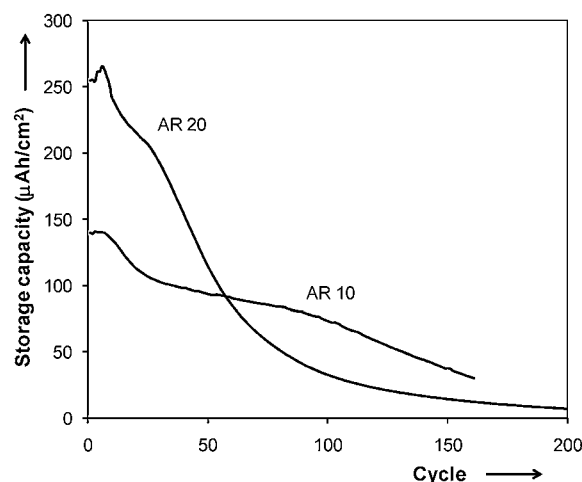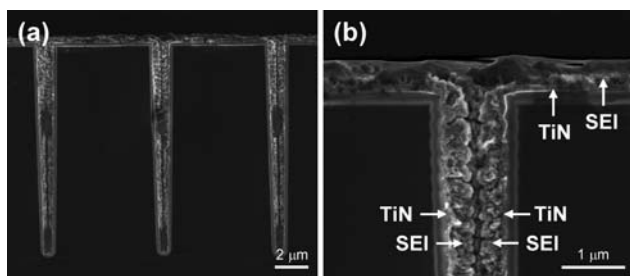

Fig. 5 First two galvanostatic cycles of poly-Si electrode deposited into aspect ratio 20 pores. Cycling is performed at 25 µA cm^{-2} between 0 and 3 V *vs.* Li/Li$^+$.

Fig. 7 Cycle life of TiN/poly-Si stacks deposited into aspect ratio pores 10 and 20 measured at 25 µA cm^{-2} between 0 and 3 V *vs.* Li/Li$^+$.

Fig. 8 SEM photographs showing an electrode stack (ALD TiN – LPCVD poly-Si) deposited inside aspect ratio 10 pores after 10 cycles. (a) Cross-section showing several complete pores and (b) magnification at the entrance of a pore. The defects observed in (a) near the centre and bottom of the pores are resulting from the sample cleavage. Note the different magnifications.

prepared using the same deposition conditions presented a longer cycle life, a capacity decline was also observed.[4,9] This decline was attributed to the continuous growth of the solid electrolyte interphase (SEI) layer, as evidenced by *ex situ* SEM of cycled electrodes.[4,9] In the present case, the continuous growth of the SEI can be even more detrimental as the pore diameter (about 1 micron) is small in comparison with the SEI layer thickness (up to several microns).[4,9]

In order to verify whether the SEI growth is responsible for the capacity decay, an electrode of aspect ratio 10 pores was cycled 10 times and inspected with SEM (Fig. 8). The TiN layer is well visible but the poly-Si thin film cannot be clearly distinguished as was also found for planar poly-Si thin film electrodes.[4,9] Moreover, it is clear that a porous SEI layer was formed on the top surface as well as inside the pores. Most of the pore volume is now occupied by SEI but the center of the pores still appear open (Fig. 8b). This open volume allows the liquid electrolyte to penetrate the pores and explains why the electrode material is still electrochemically active. After prolonged cycling, however, it can be expected that the SEI growth will completely close the pores. As a result, the kinetics of the electrochemical reaction will become severely limited and the storage capacity will decline. In order to circumvent capacity degradation, planar poly-Si thin films were successfully covered by a solid-state electrolyte and as a result the capacity retention was greatly enhanced.[4,9] Therefore, it is expected that poly-Si deposited inside these pores will also benefit from being covered by a solid-state electrolyte. However, achieving the conformal deposition of a solid-state electrolyte material inside 3D structures is a challenge that will be addressed in our future work.

The improvement of the poly-Si film morphology was demonstrated by using wide trenches (*cf.* Fig. 4). Moreover, depositing more poly-Si material inside pores can also result in the deposition of uniform thicker layers as islands similar to those observed in Fig. 2 would form a uniform layer. These improvements can be beneficial to increase the overall storage capacity of the electrode material. Another method to increase the overall storage capacity can consist of increasing the effective surface area of the substrate. This enhancement could be achieved by modifying the design parameters of the photolithographic mask. Indeed, increasing the diameter of the pores to 2 μm while keeping the same vertical and horizontal pitches, and

the same deposition conditions, would easily lead to an overall increase of the storage capacity with respect to planar films by more than a factor of 8.5.[9] Obviously, improving the step coverage of poly-Si by means of longer deposition times and decreasing the vertical and horizontal pitches will result in even higher enhancement factors.

Conclusions

The deposition feasibility of a highly structured negative electrode stack to be applied in future 3D-integrated batteries has been demonstrated. The stack comprises a TiN thin film, serving both as current collector and Li-barrier layer, which is covered by a poly-Si thin film as negative electrode material. Poly-Si films deposited inside pores show an 'island-like' structure, which probably results from the surface morphology and roughness of the underlying material. It was found that the step coverage of poly-Si can be considerably improved by growing TiN and poly-Si into wide trenches and results in the growth of much smoother poly-Si films. In comparison with planar films, these poly-Si films present a storage capacity increase of about 5× for the highest aspect ratio electrodes. Further optimization of the deposition conditions and 3D geometry can easily result in a Li-storage capacity increase of more than one order of magnitude with respect to planar films. The electrode cycle life appears to be limited by the continuous growth of the SEI layer inside the pores, which results from the use of a liquid electrolyte. Hence, the use of a solid-state electrolyte should be highly beneficial for enhancing the electrode cycle life, as already has been demonstrated for planar poly-Si thin film electrodes.

Acknowledgements

Notes and references

1 J.-M. Tarascon and M. Armand, *Nature*, 2001, **414**, 359.
2 M. Armand and J.-M. Tarascon, *Nature*, 2008, **451**, 652.
3 P. H. L. Notten, F. Roozeboom, R. A. H. Niessen and L. Baggetto, *Adv. Mater.*, 2007, **19**, 4564.
4 L. Baggetto, R. A. H. Niessen, F. Roozeboom and P. H. L. Notten, *Adv. Funct. Mater.*, 2008, **18**, 1057.
5 J. W. Long, B. Dunn, D. R. Rolison and H. S. White, *Chem. Rev.*, 2004, **104**, 4463.
6 D. Golodnitsky, M. Nathan, V. Yufit, E. Strauss, K. Freedman, L. Burstein, A. Gladkich and E. Peled, *Solid State Ionics*, 2006, **177**, 2811.
7 S. K. Cheah, E. Perre, M. Rooth, M. Fondell, A. Hårsta, L. Nyholm, M. Boman, T. Gustafsson, J. Lu, P. Simon and K. Edström, *Nano Lett.*, 2009, **9**, 3230.
8 H.-S. Min, B. Y. Park, L. Taherabadi, C. Wang, Y. Yeh, R. Zaouk, M. J. Madou and B. Dunn, *J. Power Sources*, 2008, **178**, 795.
9 L. Baggetto, J. F. M. Oudenhoven, T. van Dongen, J. H. Klootwijk, M. Mulder, R. A. H. Niessen, M. H. J. M. de Croon and P. H. L. Notten, *J. Power Sources*, 2009, **189**, 402.

10 F. Roozeboom, R. Elfrink, T. G. S. M. Rijks, J. Verhoeven, A. Kemmeren and J. van den Meerakker, *Int. J. Microcircuits Electron. Packag.*, 2001, **24**, 182.
11 H. C. M. Knoops, L. Baggetto, E. Langereis, M. C. M. van de Sanden, J. H. Klootwijk, F. Roozeboom, R. A. H. Niessen, P. H. L. Notten and W. M. M. Kessels, *J. Electrochem. Soc.*, 2008, **155**, G287.
12 H. C. M. Knoops, M. E. Donders, L. Baggetto, M. C. M. van de Sanden, P. H. L. Notten and W. M. M. Kessels, *ECS Trans.*, 2009, **25**, 333.
13 S. B. S. Heil, J. L. Hemmen, C. J. Hodson, N. Singh, J. H. Klootwijk, F. Roozeboom, M. C. M. van de Sanden and W. M. M. Kessels, *J. Vac. Sci. Technol., A*, 2007, **25**, 1357.
14 D. Hoogeland, K. B. Jinesh, F. C. Voogt, W. F. A. Besling, Y. Lamy, F. Roozeboom, M. C. M. van de Sanden and W. M. M. Kessels, *ECS Trans.*, 2009, **25**, 389.
15 C. Amatore, A. I. Oleinick and I. Svir, *Anal. Chem.*, 2009, **81**, 4397.